Appendix N 4/23/10

The Atmospheric Effects of HSCT Emissions Simulated by a 3-wave Interactive Model

R.-L. Shia, M.K.W. Ko and N.D. Sze

The Atmospheric Effects of HSCT Emissions Simulated by a 3-wave Interactive Model

R.-L. Shia, M. K. W. Ko, and N. D. Sze

AER Inc., 840 Memorial Dr. Cambridge, MA 02139

10/99

Abstract

An interactive model which couples a semi-spectral dynamical model, a radiative transfer code and a two-dimensional chemistry transport model (2-D CTM), is used to assess the atmospheric effects of the High-Speed Civil Transport (HSCT) engine emissions. The residual mean meridional circulation, the zonal-mean temperature and the eddy diffusion coefficients are calculated using zonal means and three longest zonal waves of dynamical variables integrated in the semi-spectral dynamical model. They are used in the 2-D CTM to simulate the distribution of trace gases in the atmosphere. The simulated ozone is sent to the radiative transfer code to calculate the heating rates, which drive the dynamics. This radiative coupling connects the dynamical and photochemical processes and creates feedback when the atmosphere is perturbed.

It is found that in most areas the ozone depletion caused by HSCT emissions calculated using the 3-wave model has the features similar to, but with significantly larger magnitude than that calculated by the AER 2-D CTM with prescribed transport parameters and temperature. The difference is mostly due to the differences in the circulation in the two models. The radiative feedback effects are investigated by comparing the ozone depletion calculated with the baseline dynamics and with the dynamics perturbed by the HSCT emissions. The feedback through changes in the residual mean meridional circulation and the eddy diffusion coefficients has moderate effects on the simulated ozone depletion. It reduced the ozone depletion by 20-30% in northern mid and high-latitudes. However, the feedback through changes in the zonal-mean temperature is negligible.

1. Model Description and Simulation of the Background Atmosphere

The 3-wave model has three components, a semi-spectral dynamical model, a radiative transfer code, and a 2-D CTM. The theoretic framework of the dynamical model is adopted from Schneider and Geller (1984). The model is developed from the AER 2-D interactive model (Ko, et al., 1993). It is formulated using the primitive equations and the vertical coordinate is $z = H*\ln(p_0/p)$. The zonal mean radiative heating rates are calculated every 10 days using a narrow-band radiative transfer scheme described by Wang and Ryan (1983). The chemistry scheme from the AER two-dimensional chemical transport model (Ko et al. 1984, 1985, 1989; Weisenstein et al. 1993) is used to calculate the chemical source term and loss rates. The heterogeneous reactions on the surfaces of the sulfite aerosols are included in the calculations. The model has 9.5° resolution in latitude (19 boxes from pole to pole), ~3.5 km resolution in altitude (half scale height), and the three longest zonal waves are calculated in the dynamical module. The 2-D CTM has 17 vertical layers (from the surface to ~60 km) while the dynamical module includes seven extra layers to place the upper boundary at ~84 km.

The 3-wave model differs from the AER 2-D interactive models in that it uses a highly truncated three-dimensional dynamical module to calculate the zonal mean and three longest zonal waves of dynamical variables. From these dynamical fields a residual circulation and eddy diffusion coefficients for chemical tracer are derived to represent the meridional transport. They are used in the 2-D CTM along with the zonally averaged temperature to distribute the chemical composition of the atmosphere. The interactions between the dynamical and photochemical processes are achieved through the radiative coupling when the model-calculated O_3 is used to compute the radiative heating rates, which is the driving force of the dynamics. The data flow chart of the model is shown in Fig. 1. Following the arrows in the diagram, interactions and feedback between the dynamical, radiative and photochemical processes are easily identified. The data are exchanged between the dynamical model, the radiative transfer code and the 2-D CTM every ten days.

In spite of the high truncation in the dynamical module (only three longest waves are resolved), the model has simulated many observed characteristics of stratospheric dynamics and distribution of chemical species including ozone. The month-latitude

distribution of O_3 column abundance from the model results and from TOMS data are plotted in Fig. 2. The ozone column abundance from model simulation for present day atmosphere (Fig. 2 a) shows a strong hemispheric asymmetry. The general features of the O_3 column distribution are similar to the observations from Total Ozone Mapping Spectrometer (TOMS), which are shown in Fig. 2 b. The modeled spring maximum in both hemispheres appears in the right places with more or loss right amplitudes but a little later in time. The calculated ozone column abundance in the northern mid- and high-latitudes during late summer and fall is about 40-60 Dobson Unit (D. U.) higher than the observations.

Compared with the values commonly used in 2-D CTMs, the eddy diffusion coefficients for chemical species calculated in this model are smaller, especially in the subtropics. Also the calculated residual circulation is weaker than that used in AER 2-D CTM. The detailed model descriptions and the simulations for current atmosphere can be found in Shia et al. (1999).

2. Ozone Response to the High-Speed Civil Transport (HSCT) Engine Emissions

The atmospheric effects of a HSCT fleet of 500 supersonic airplanes with NO_y emission index EI=15, and the speed Mach=2.4 is assessed using both the 3-wave interactive model and the AER 2-D CTM. The AER 2-D CTM has been modified recently to install a tropical pipe (Weisenstein, et al., 1996). The tropical pipe is surrounded by a subtropical barrel, which substantially slows the exchange between the tropics and the mid-latitudes in the stratosphere. The barrel is parameterized in the model by reducing the horizontal eddy diffusion coefficient from 3.0 to 0.3 $x10^5$ m^2/s.

The atmospheric effects of the HSCT usually are measured by the ozone depletion, the percent change of the ozone column abundance caused by the HSCT engine emissions. In order to compare assessment results of the AER 3-wave model and the 2-D CTM, the model runs listed in Table 1 are completed. The off-line runs of the 3-wave model are executed similar to the 2-D CTM, where the transport and temperature are prescribed instead of being calculated. In Table 1 and all following tables the prescribed fields are put inside parentheses. From the model runs listed in Table 1, the simulated ozone depletions are plotted in Fig. 3. The ozone depletions simulated by the AER 2-D CTM without the tropical pipe (the percent change of ozone column density

between the Case A and Case B) and with the tropical pipe (Case C and Case D) are plotted in Fig. 3a and 3b, respectively. The ozone depletions simulated by the 3-wave model with full feedback (the percent change of ozone column density between the Case E and Case F) and without feedback (Case G and Case H) are plotted in Fig. 3c and 3d, respectively. The Fig 3c and 3d show that the feedback is negative (reducing the perturbation in ozone). We will discuss more about the feedback effects in the next section. Comparing the Fig. 3 c and 3a, it is found that although they have the similar shape, in the northern mid- and high-latitudes the ozone depletion in the 3-wave model simulation is about 2 to 3 times larger than that in the 2-D CTM simulation. In the tropics, HSCT engine emissions actually increase the ozone column abundance in 3-wave model simulation by less than 0.4 % (Fig. 3c). A similar result is found in the simulation of the 2-D CTM with the tropical pipe (Fig. 3b).

The differences in the ozone depletions assessed by the 2-D CTM and 3-wave model have two origins. The first is the differences in the redistribution of HSCT engine emissions after they are deposited in the middle atmosphere due to the different transport and temperature fields in the two models. Through chemical reactions, different emission distributions will produce different ozone depletion. In addition to that, even if the final distribution of the HSCT emissions remains the same, because of the differences in the transport and temperature the ozone distributions simulated by the two models can be quite different and so the ozone depletion. The Table 2 lists the model runs used to show how the stream function, temperature and eddy diffusion coefficient calculated in 3-wave model effect the redistribution of engine emissions individually. The increases of NO_y in January caused by the HSCT engine emissions simulated using 3-wave model are plotted in Fig. 4a. The increases of NO_y in January caused by the HSCT engine emissions simulated using mixed 3-wave and 2-D CTM dynamics are plotted in Fig. 4b-4d. Also the increases of NO_y in January caused by the HSCT engine emissions simulated using 2-D CTM with and without the tropical pipe are plotted in Fig. 4e and 4f, respectively. The weaker eddy diffusion calculated by the 3-wave model reduces the dispersion of the engine emissions and limits them mainly in the Northern Hemisphere (Fig. 4 d). It is worth to notice that the global averages of the increases of NO_y in January caused by the HSCT engine emissions for Fig. 4a –4f are 0.153, 0.150, 0.122, 0.106, 0.115, and 0.113 D.U., respectively. The weaker circulation calculated by the 3-wave model reduces the flux of engine emissions into the troposphere and increases their concentration in the stratosphere to 1.50 D.U. (Fig. 4 b) from 0.115 D.U. (Fig. 4e)

As mentioned above, the changes in the ozone depletions assessed by different models with the same photochemistry module have two origins: the changes in the emission distributions due to the different dynamics in the models and the different ozone response to the different model dynamics under the same distribution of engine emissions. The Table 3 lists the off-line runs completed with fixed engine emission distributions so we can study the second origin, the ozone response. All the off-line runs in the Table 3 use the fixed distributions for NO_y, CH_4, H_2O and CO, the main active component of the engine emissions, calculated in the 2-D CTM with the tropical pipe, i.e. Case C for HSCT and Case D for subsonic only in Table 1. The ozone depletions simulated using the total dynamics of the 3-wave model, its stream function only, its temperature only and its eddy diffusion coefficients only, with the emission distributions fixed are plotted in Fig. 5 respectively. The ozone depletion using the 3-wave model stream function only (Fig. 5 b) is closest to the ozone depletion using the total dynamics of the 3-wave model (Fig. 5 a). In contrast, the ozone depletion using the 3-wave model temperature (Fig. 5 c) is very close to the ozone depletion calculated in the 2-D CTM with the tropical pipe (Fig. 3b). The ozone depletion using the total dynamics of the 3-wave model with the fixed emission distributions (Fig. 5a) is close to the ozone depletion simulated by the 3-wave model (Fig. 3d). This means that the differences in the ozone depletion between the 3-wave model and the 2-D CTM are mainly due to the different ozone transport, the second origin, especially the advection, in the two models not the differences in the distributions of the engine emissions.

3. Feedback Effects in 3-Wave model

When the HSCT supersonic airplanes fly in the atmosphere, their engine emissions change the composition of the air, especially the ozone distribution, which is important for determining the radiative heating. The radiative heating rates supply the energy for the atmospheric dynamics. Therefore, the ozone changes caused by HSCT engine emissions could alter the transport and the temperature in the atmosphere and the changed dynamics should generate a different ozone distribution (See Fig. 1 for the interactions between the components of the 3-wave model). This is the radiative feedback of the ozone depletion. Up to now we only have discussed the 3-wave model runs with the dynamics calculated for subsonic only, (i. e. ψ^0, T^0, K^0_{yy}, unperturbed dynamics), and therefore, no feedback has been included. In this paragraph, we use the model results from runs listed in Table 4 to estimate the effects of the radiative feedback. These runs for HSCT cases use the dynamics perturbed by HSCT emissions (i. e. ψ^S,

T^S, K_{yy}^S generated in case E in Table 1) or part of it and the runs with subsonic only cases use unperturbed dynamics (i. e. ψ^0, T^0, K_{yy}^0). The feedback effects of ozone depletion through the changes in the stream function, the temperature and eddy diffusion coefficients individually or collectively are shown in Fig. 6. All cases used in Fig. 6 have the HSCT source. The Fig. 6 a) is the column ozone difference between the full interactive run and run with unperturbed dynamics. This ozone column difference is caused by the full feedback. The feedback reduces the ozone depletion, (compared with Fig. 3 d, the ozone depletion without feedback, where the ozone reduction is about 6-8 D.U. in northern midlatitudes), by 20 to 30 %, which is a moderate negative feedback. Fig. 6 b)-d) show the ozone changes caused by partial feedback, through the stream function, the temperature, and the eddy diffusion coefficients, respectively. The feedback through the change in the stream function is most important (Fig. 6 b), and the feedback through the change in the temperature is negligible (Fig. 6 c).

4. Conclusions and Discussions

We have reached the following conclusions in this study:

1. Ozone depletion caused by HSCT engine emissions in the northern mid- and high-latitudes is significantly larger in 3-wave model simulations than in 2-D CTM. In the tropics, HSCT engine emissions increase the ozone column abundance in 3-wave model simulations, similar to 2-D CTM with the tropical pipe.

2. The differences of the ozone depletion caused by HSCT engine emissions between 3-wave model and 2-D CTM are largely due to differences in the ozone transport.

3. The feedback due to changes in dynamics of the 3-wave model in calculating the ozone response to HSCT engine emissions is negative. The feedback reduces the ozone depletion in northern mid- and high-latitudes by 20-30%, mainly by the feedback due to changes in circulation.

The calculated ozone column abundance in the present day atmosphere (Fig. 2 a) in the northern high latitudes during fall is about 40 to 60 Dobson Unit higher than observation (Fig. 2 b). Because the problem is limited in northern high latitude for a

short period, we don't expect the remedy of this problem would change the conclusions listed above in any significant ways.

Acknowledgments. The supports of NASA Office of Mission to Planet Earth Science Division (Contract NASW-4775), NASA Atmospheric Chemistry Modeling and Analysis Program (NAS5-97039) and by MASA Atmospheric Effect of Aviation Program (NAS5-32371) are gratefully acknowledged.

Table 1 Model Runs for Ozone Depletion

	HSCT (Mach=2.4; EI=15; 500)	Subsonic only
2-D CTM (no pipe)	Case A (ψ^{2D}, T^{2D}, K_{yy}^{NP})	Case B (ψ^{2D}, T^{2D}, K_{yy}^{NP})
2-D CTM (pipe)	Case C (ψ^{2D}, T^{2D}, K_{yy}^{P})	Case D (ψ^{2D}, T^{2D}, K_{yy}^{P})
3-Wave Model (interactive)	Case E ψ^{S}, T^{S}, K_{yy}^{S}	Case F ψ^{0}, T^{0}, K_{yy}^{0}
3-Wave Model (off-line)	Case G (ψ^{0}, T^{0}, K_{yy}^{0})	Case H (ψ^{0}, T^{0}, K_{yy}^{0})

where ψ^{2D}, T^{2D}, K_{yy}^{NP} are the stream functions, temperature fields and the eddy diffusion coefficients prescribed in the 2-D CTM without tropical pipe; ψ^{0}, T^{0}, K_{yy}^{0} and ψ^{S}, T^{S}, K_{yy}^{S} are the stream functions, temperature fields and the eddy diffusion coefficients calculated in the 3-wave model without and with HSCT emissions respectively. K_{yy}^{P} is the eddy diffusion coefficients prescribed in the 2-D CTM with the tropical pipe. The off-line runs of 3-wave model are executed just like 2-D CTM. It is worth to notice that case F, which is a interactive run, and case H, which is a off-line run, produce the same tracer distributions because they have the same transport and temperature to drive the 2-D CTM.

Table 2. Model Runs for ΔNO_y Due to HSCT

	HSCT	Subsonic only
3-Wave Model (off-line)	Case 1 (ψ^0, T^{2D}, K_{yy}^{NP})	Case 2 (ψ^0, T^{2D}, K_{yy}^{NP})
3-Wave Model (off-line)	Case 3 (ψ^{2D}, T^0, K_{yy}^{NP})	Case 4 (ψ^{2D}, T^0, K_{yy}^{NP})
3-Wave Model (off-line)	Case 5 (ψ^{2D}, T^{2D}, K_{yy}^0)	Case 6 (ψ^{2D}, T^{2D}, K_{yy}^0)

Table 3. Model Runs with Fixed NO_y, CH_4, H_2O and CO

	HSCT	Subsonic only
2-D CTM (pipe)	Case C $(\psi^{2D}, T^{2D}, K_{yy}^{P})$ NO_X^S ...	Case D $(\psi^{2D}, T^{2D}, K_{yy}^{P})$ NO_X^0...
3-Wave Model (off-line)	Case 7 $(\psi^{0}, T^{0}, K_{yy}^{0})$ $(NO_X^S...)$	Case 8 $(\psi^{0}, T^{0}, K_{yy}^{0})$ $(NO_X^0...)$
3-Wave Model (off-line)	Case 9 $(\psi^{0}, T^{2D}, K_{yy}^{P})$ $(NO_X^S...)$	Case 10 $(\psi^{0}, T^{2D}, K_{yy}^{P})$ $(NO_X^0...)$
3-Wave Model (off-line)	Case 11 $(\psi^{2D}, T^{0}, K_{yy}^{P})$ $(NO_X^S...)$	Case 12 $(\psi^{2D}, T^{0}, K_{yy}^{P})$ $(NO_X^0...)$
3-Wave Model (off-line)	Case 13 $(\psi^{2D}, T^{2D}, K_{yy}^{0})$ $(NO_X^S...)$	Case 14 $(\psi^{2D}, T^{2D}, K_{yy}^{0})$ $(NO_X^0...)$

NO_X^S ... and NO_X^0... are the distributions for chemical species included in the HSCT engine emissions simulated using the AER 2-D CTM with the tropical pipe with and without the HSCT input, respectively.

Table 4. Model Runs for Feedback Effects

	HSCT
3-Wave Model (off-line)	Case 15 (ψ^0, T^S, K_{yy}^S)
3-Wave Model (off-line)	Case 16 (ψ^S, T^0, K_{yy}^S)
3-Wave Model (off-line)	Case 17 (ψ^S, T^S, K_{yy}^0)

Figure Captions

Fig. 1 The flow chart of the 3-wave interactive model. The arrows indicate the direction of data flow. The data exchange represents the interactions between the different components of the model. The loops formed by arrows represent feedback routes.

Fig. 2 Latitude-time cross section of ozone column abundance (D. U.) from a) 3-wave model simulation for present day, b) TOMS measurements. The contour increment is 20 D. U.

Fig. 3 The ozone depletion caused by HSCT engine emissions, (Mach=2.4, EI=15, with a fleet of 500 airplanes), simulated by a) AER 2-D CTM without the tropical pipe (case A - case B), b) AER 2-D CTM with the tropical pipe (case C - case D), c) AER 3-wave interactive model with feedback (case E - case F), d) AER 3-wave interactive model without feedback (case G - case H). The contour levels are -5, -3, -2, -1.5, -1, -0.5, -0.2, 0, 0.2, 0.5 (%).

Fig. 4 The increases of NO_y in January caused by HSCT engine emissions, (Mach=2.4, EI=15, with a fleet of 500 airplanes), simulated using a) 3-wave model (case G - case H in Table 1), b) 3-wave model's stream function with temperature and K_{yy} from AER 2-D CTM without the tropical pipe (case 1 - case 2 in Table 2), c) 3-wave model's temperature with stream function and K_{yy} from AER 2-D CTM without the tropical pipe (case 3 - case 4 in Table 2), d) 3-wave model's K_{yy} with temperature and stream function from AER 2-D CTM without the tropical pipe (case 5 - case 6 in Table 2), e) AER 2-D CTM without the tropical pipe, and f) AER 2-D CTM with the tropical pipe. The contour increment is 1 pptv.

Fig. 5. The ozone depletion caused by HSCT engine emissions, (Mach=2.4, EI=15, with a fleet of 500 airplanes), simulated with fixed distributions for NO_y, CH_4, H_2O and CO from the AER 2-D CTM with the tropical pipe and dynamics from a) the 3-wave model (case 7 - case 8 in Table 3), b) 3-wave model's stream function with temperature and K_{yy} from AER 2-D CTM with the tropical pipe (case 9 - case 10 in Table 3), c) 3-wave model's temperature with stream function and K_{yy} from AER 2-D CTM with the tropical pipe (case 11 - case 12 in Table 3), d) 3-wave model's K_{yy} with temperature and stream function from AER 2-D CTM with the tropical pipe (case 13 - case 14 in Table 3). The contour levels are -5, -3, -2, -1.5, -1, -0.5, -0.2, 0, 0.2, 0.5 (%).

Fig 6. The differences between the ozone column abundance (D.U.) simulated by the interactive 3-wave model with HSCT emissions (Case E in Table 1) and the ozone column abundances simulated using off line 3-wave model with a) unperturbed dynamics (case G in Table 1), b) unperturbed stream function and perturbed temperature and K_{yy} (case 15 in Table 4), c) unperturbed temperature and perturbed stream function and K_{yy} (case 16 in Table 4), d) unperturbed K_{yy} and perturbed stream function and temperature (case 17 in Table 4), with HSCT emissions. The contour increment is 0.5 D.U.

References

Ko, M.K.W., N.D. Sze, M. Livshits, M.B. McElroy, and J.A. Pyle, 1984: The seasonal and latitudinal behavior of trace gases and O_3 as simulated by a two-dimensional model of the atmosphere. *J. Atmos. Sci.*, **41**, 2381-2408.

Ko, M.K.W., K.K. Tung, D.K. Weisenstein, and N.D. Sze, 1985: A zonal mean model of stratospheric tracer transport in isentropic coordinates: numerical simulation for nitrous oxide and nitric acid. *J. Geophys. Res.*, **90**, 2313-2329.

Ko, M.K.W., N.D. Sze and D.K. Weisenstein, 1989: The roles of dynamical and chemical processes in determining the stratospheric concentration of ozone in one-dimensional and
two-dimensional models. *J. Geophys. Res.*, **94**, 9889-9896.

Shia, Run-Lie, Shuntai Zhou, Malcolm K. W. Ko, Nien-Dak Sze,
David Salstein and Karen Cady-Pereira, 1999: A Three-Wave Model of the Stratosphere With Coupled Dynamics, Radiation and Photochemistry, submitted to *J. Atmos. Sci.*

Wang, W.-C. and P. B. Ryan, 1983: Overlapping effect of atmospheric H_2O, CO_2 and O_3 on the CO_2 radiative effect. *Tellus*, **35B**, 81-91.

Weisenstein, D. K., M. K. W. Ko, J. M. Rodriguez and N.-D. Sze, 1993: Effects on stratospheric ozone from High-Speed Civil Transport: Sensitivity to stratospheric aerosol loading. *J. Geophys. Res.*, **98**, 23,133-23140.

Weisenstein, D. K., M. K. W. Ko, N.-D. Sze, and J. M. Rodriguez, 1996: Potential impact of SO2 emissions from stratospheric aircraft on ozone, *Geophys. Res. Lett.*, **23** , pp. 161-164.

3-Wave Interactive Model

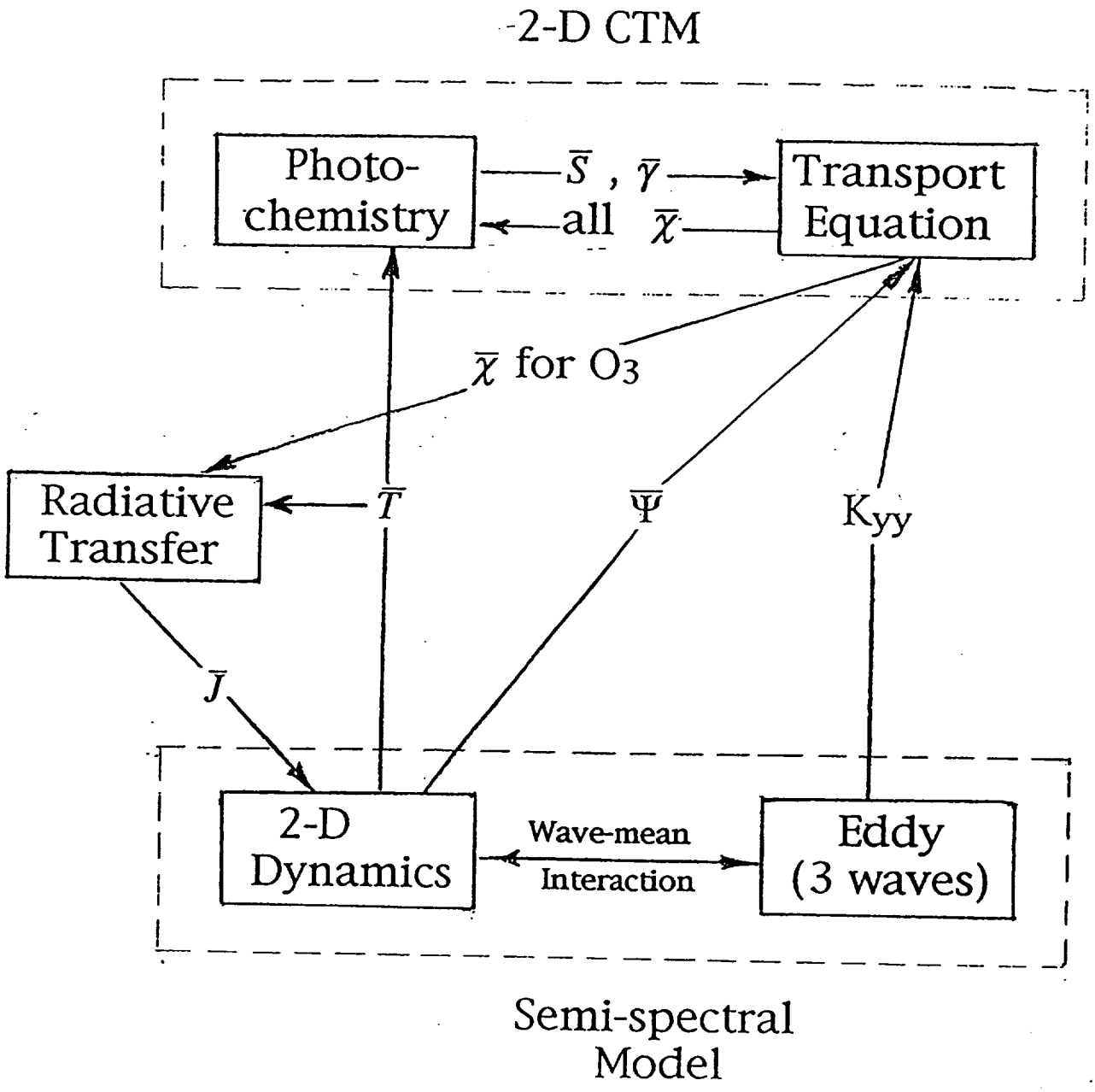

Fig. 1 The flow chart of the three-wave interactive model. The arrows indicate the direction of data flow. The loops formed by arrows represent feedbacks.

Ozone Column Abundance (D. U.)

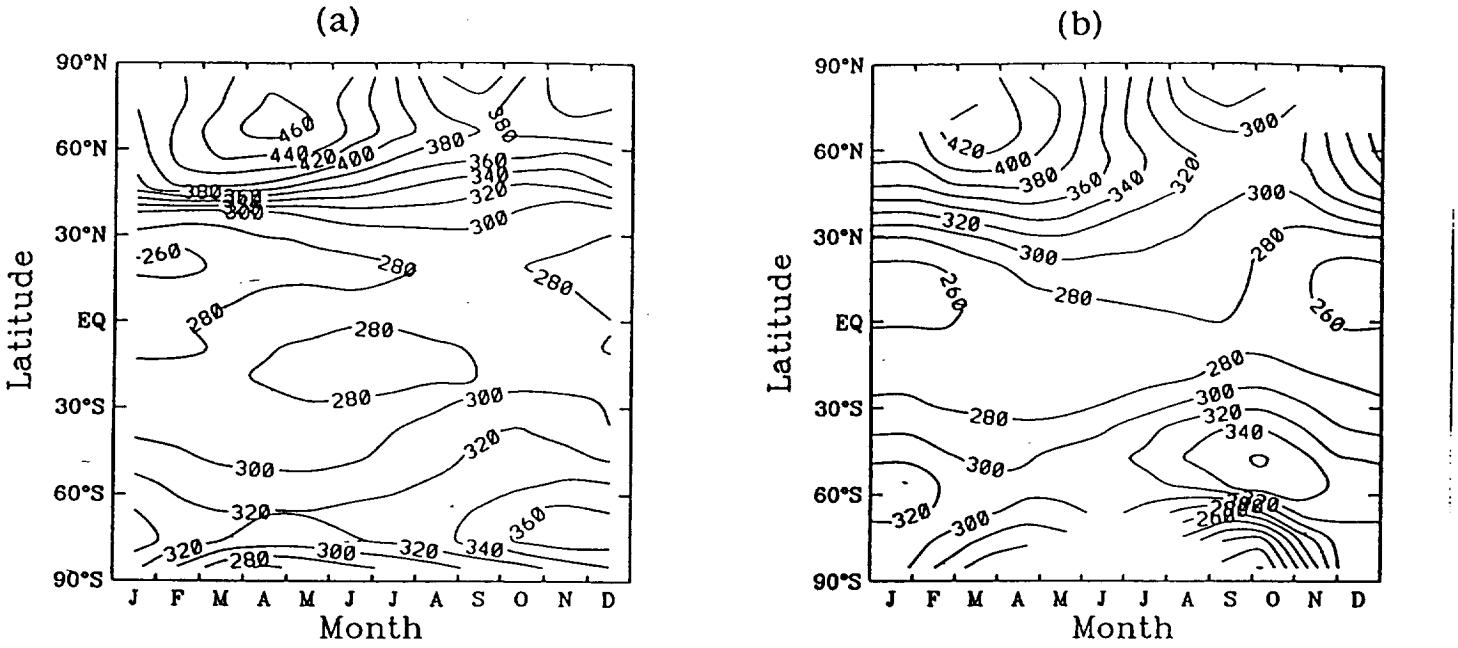

Fig. 2

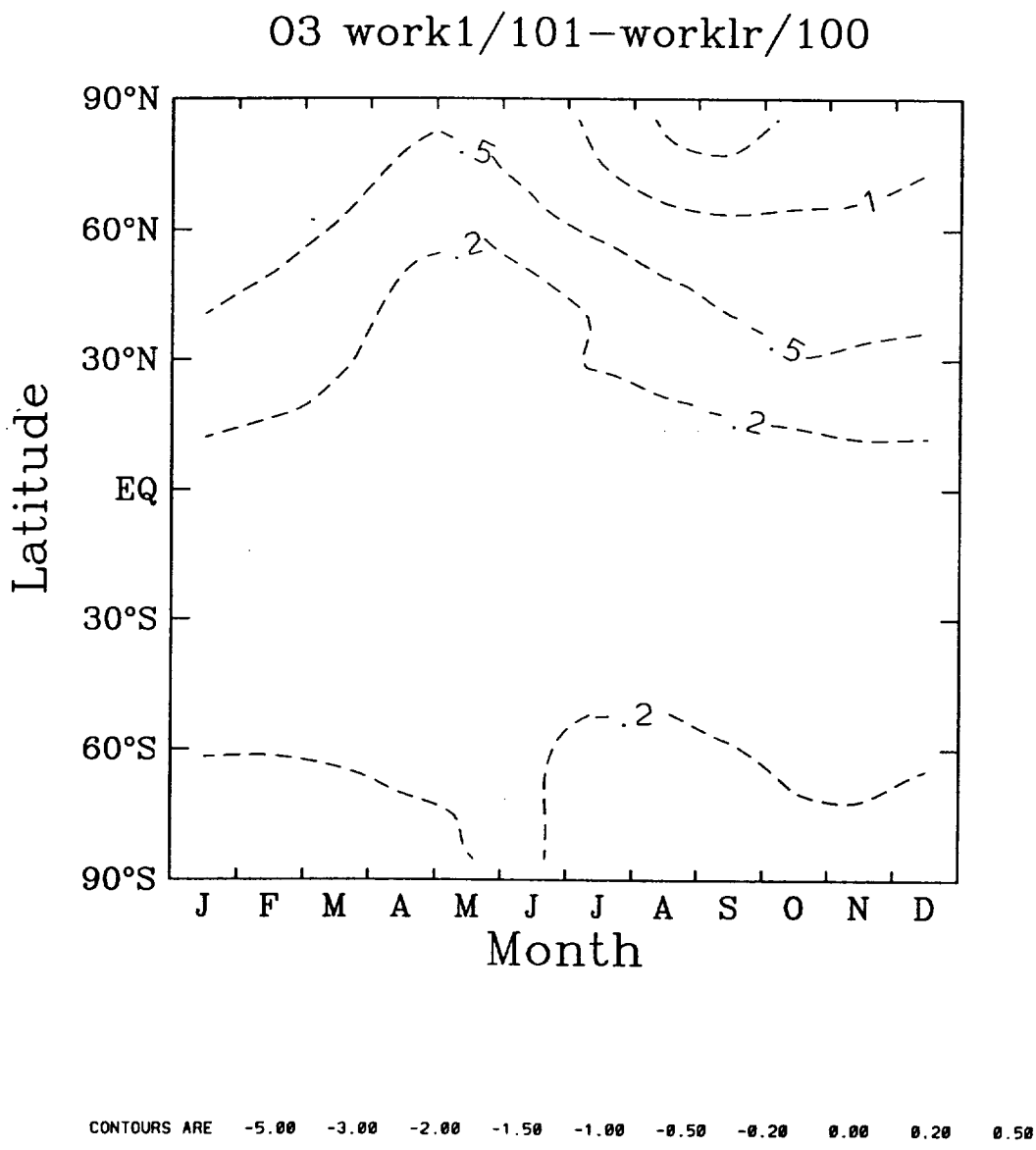

CONTOURS ARE -5.00 -3.00 -2.00 -1.50 -1.00 -0.50 -0.20 0.00 0.20 0.50

Wed Oct 13 12:51:17 EDT 1999

Fig 3a

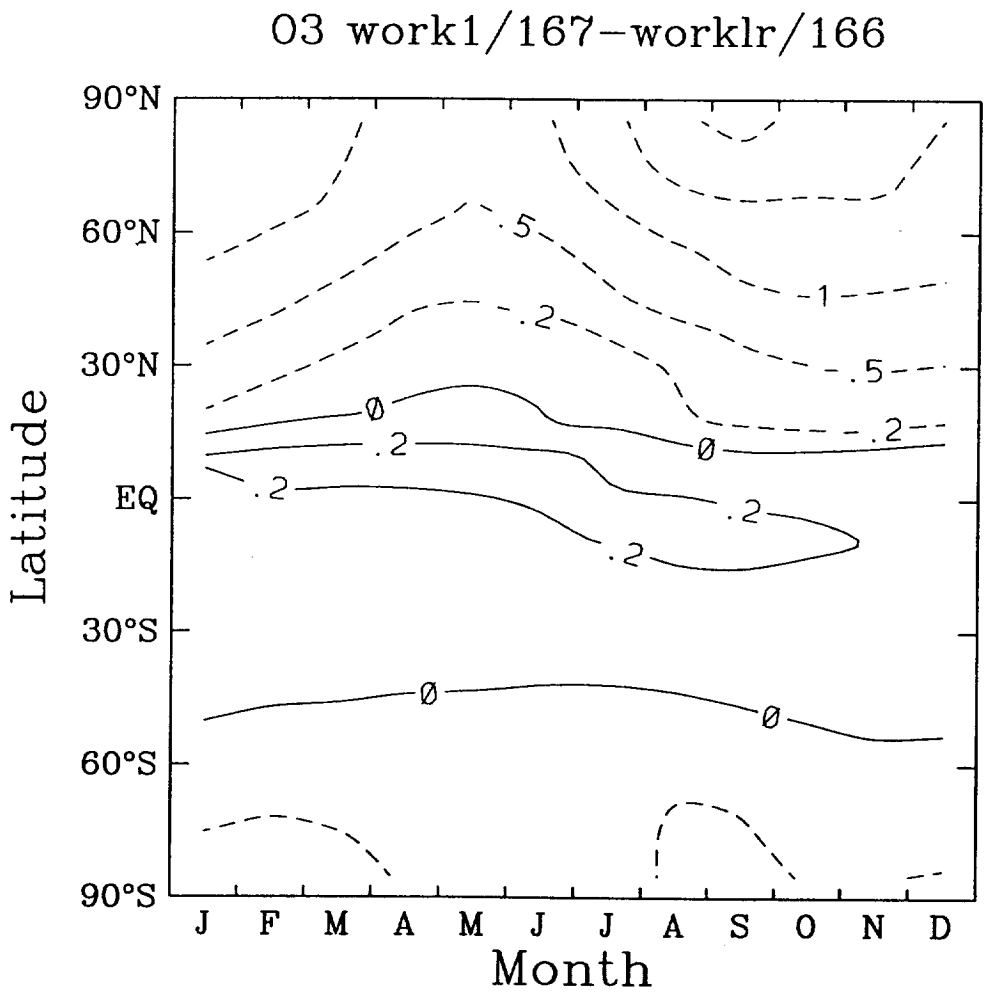

CONTOURS ARE -5.00 -3.00 -2.00 -1.50 -1.00 -0.50 -0.20 0.00 0.20 0.50

Wed Oct 13 11:35:22 EDT 1999

Fig 3.b

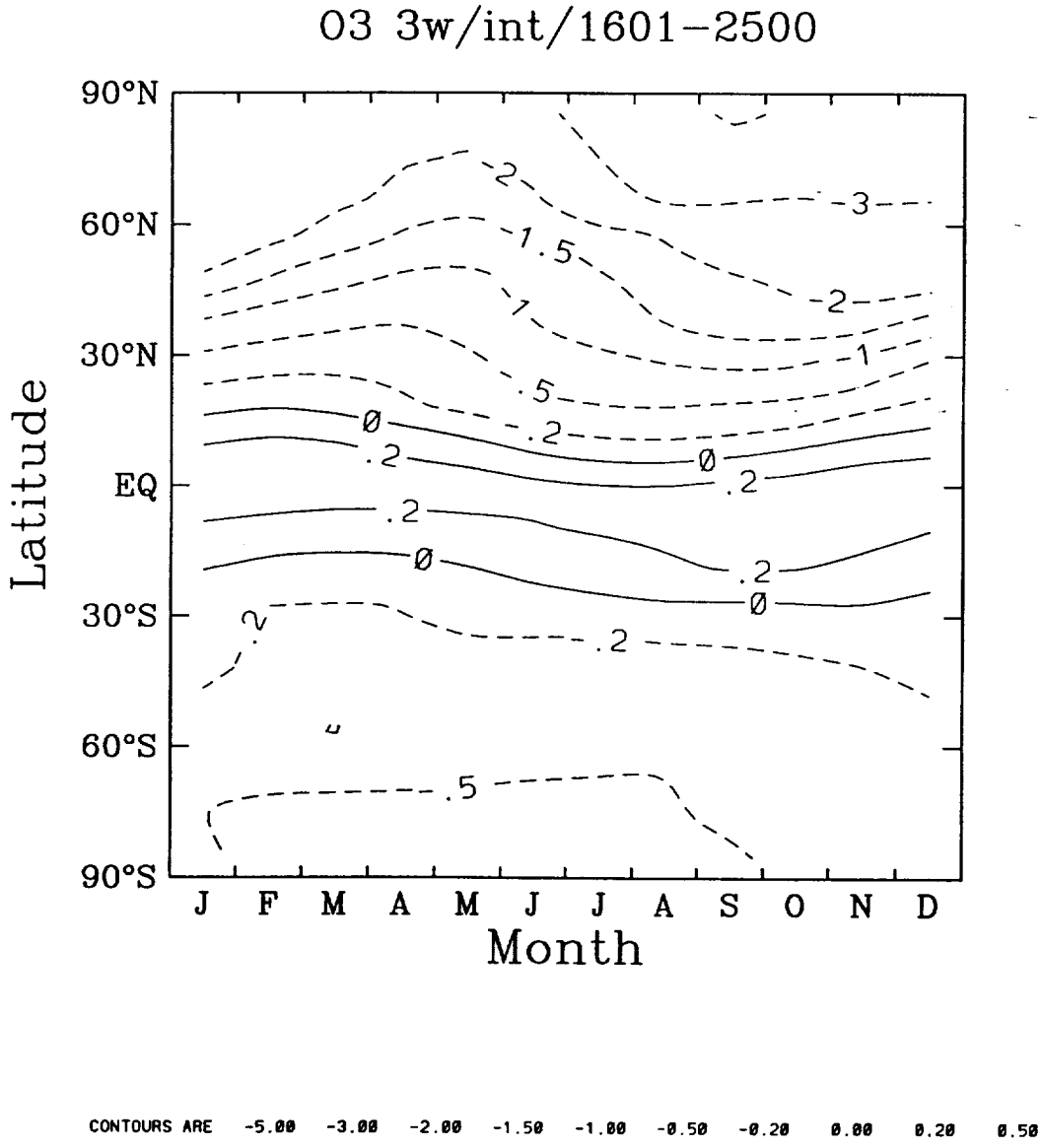

Wed Oct 13 11:39:20 EDT 1999

Fig. 3.C

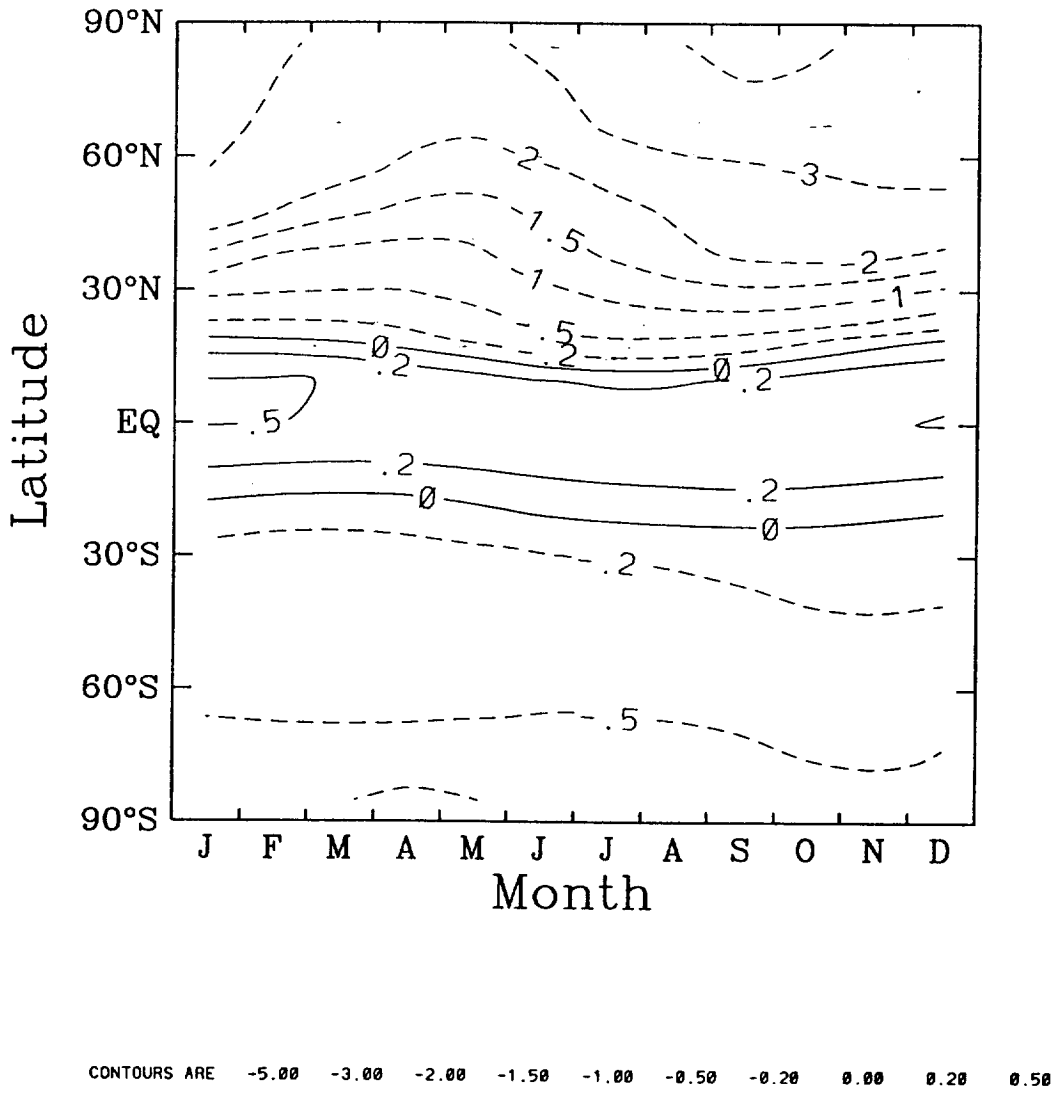

Wed Oct 13 11:40:54 EDT 1999

Fig 3d

NOx 2003–2500

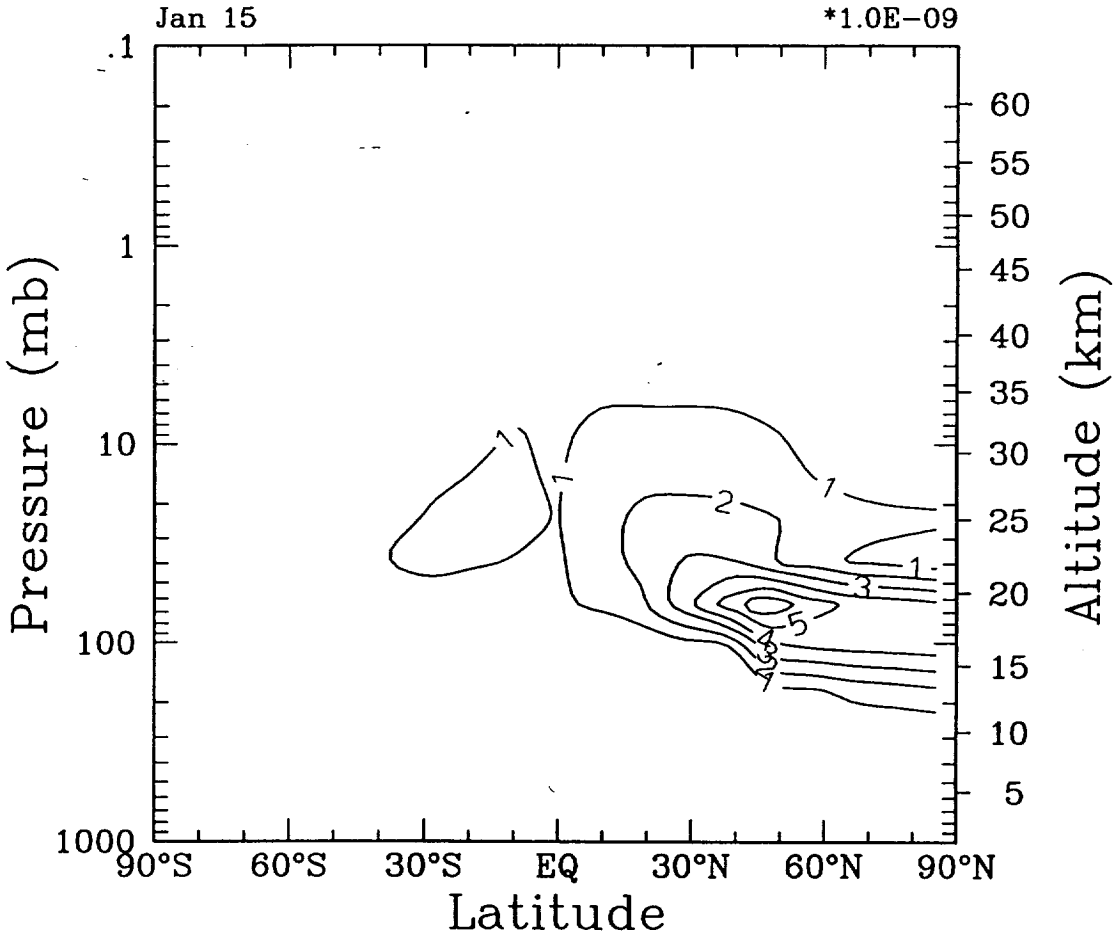

CONTOUR FROM 0. TO 10.000 CONTOUR INTERVAL OF 1.0000 PT(3,3)= 6.81470E-03

Wed Oct 13 13:03:33 EDT 1999

Fig 4a

NOx 193−192

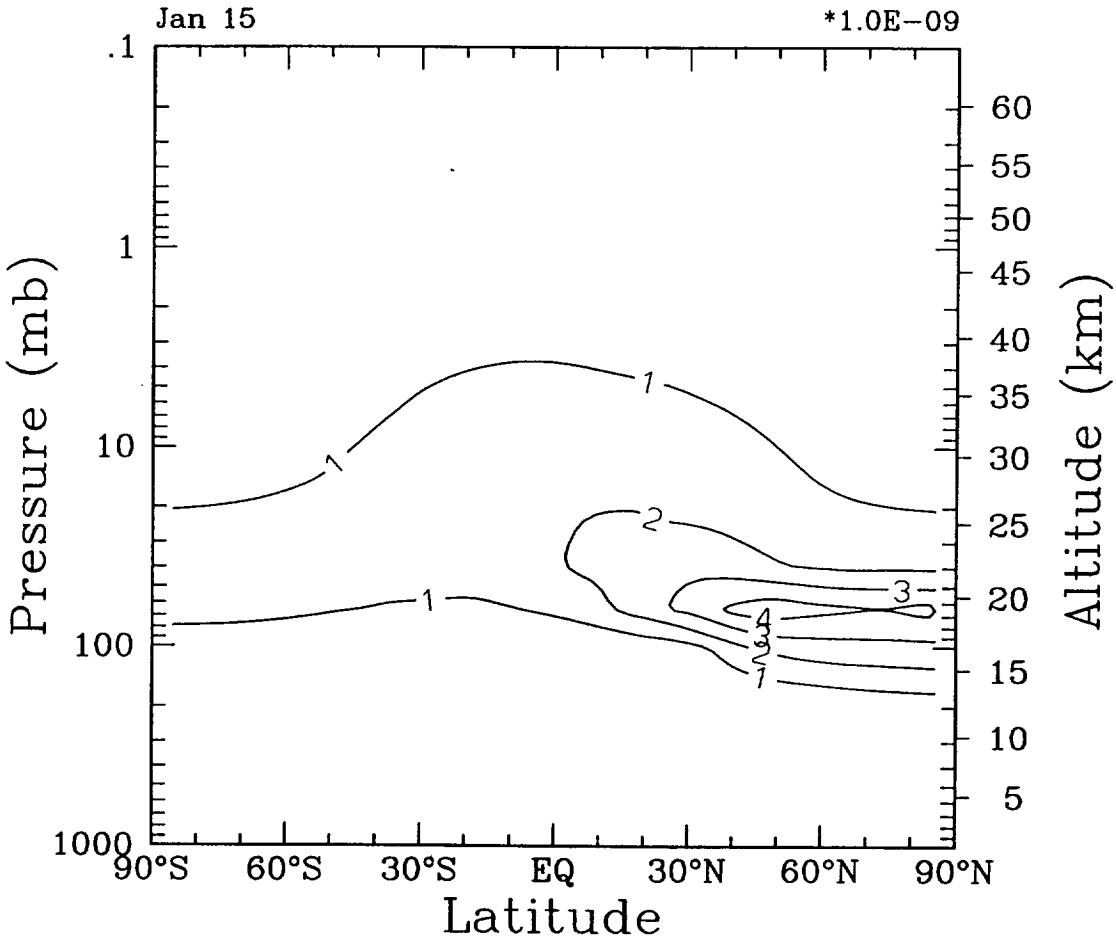

CONTOUR FROM 0. TO 10.000 CONTOUR INTERVAL OF 1.0000 PT(3,3)= 5.22173E-03

Wed Oct 13 13:01:36 EDT 1999

Fig. 4b

NOx 165−164

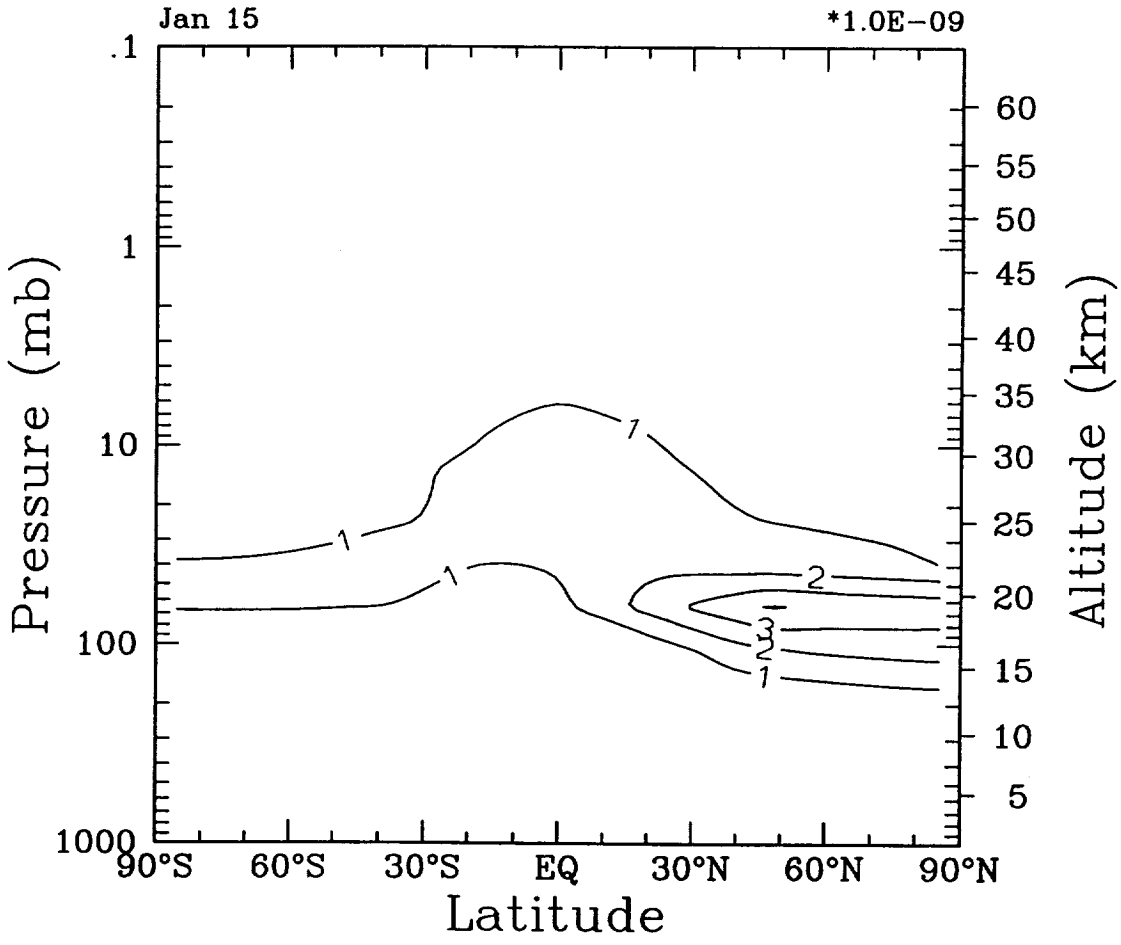

CONTOUR FROM 0. TO 10.000 CONTOUR INTERVAL OF 1.0000 PT(3,3)= 5.94775E-03

Wed Oct 13 13:00:19 EDT 1999

Fig 4c

NOx 3806-3205

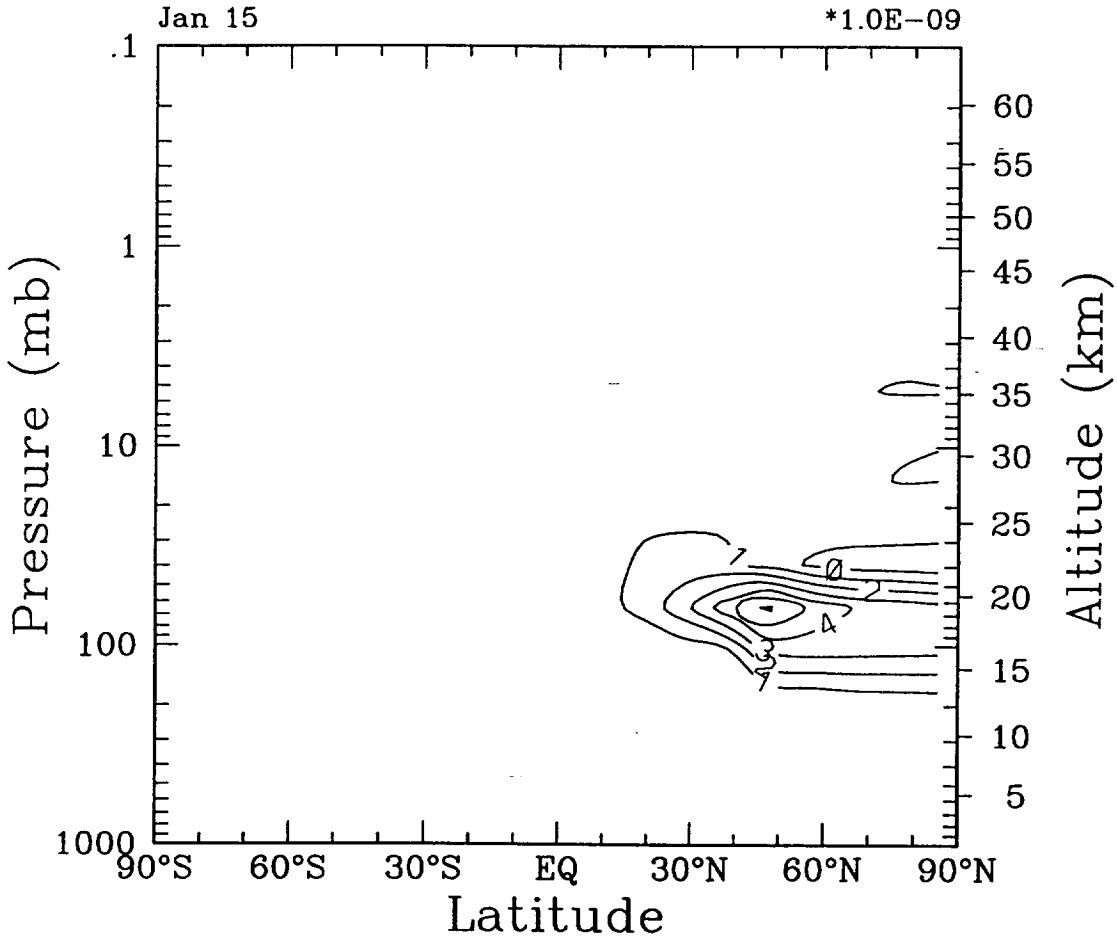

CONTOUR FROM 0. TO 10.000 CONTOUR INTERVAL OF 1.0000 PT(3,3)= 3.98191E-03

Wed Oct 13 13:05:19 EDT 1999

Fig. 4d

NOx 101−100

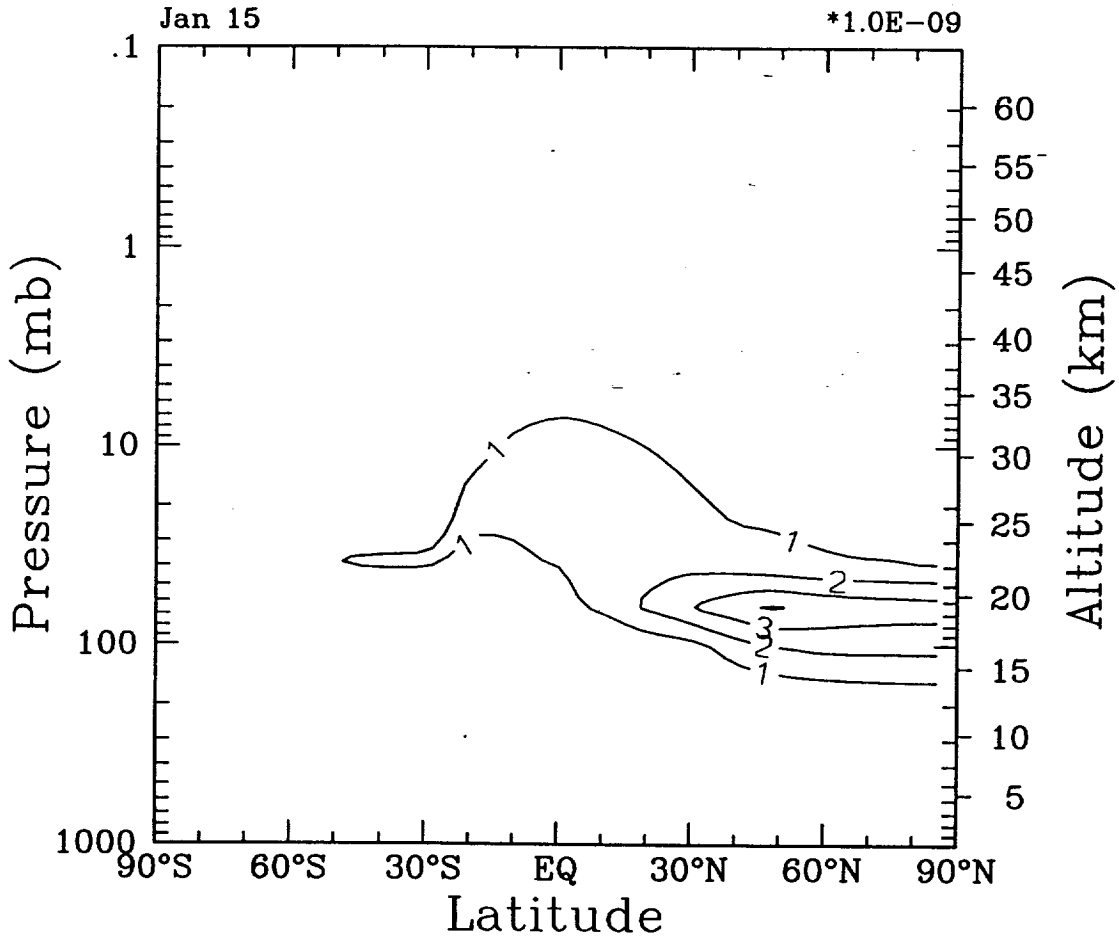

CONTOUR FROM 0. TO 10.000 CONTOUR INTERVAL OF 1.0000 PT(3,3)= 4.14298E-03

Thu Oct 14 10:37:46 EDT 1999

Fig 4e

NOx 167−166

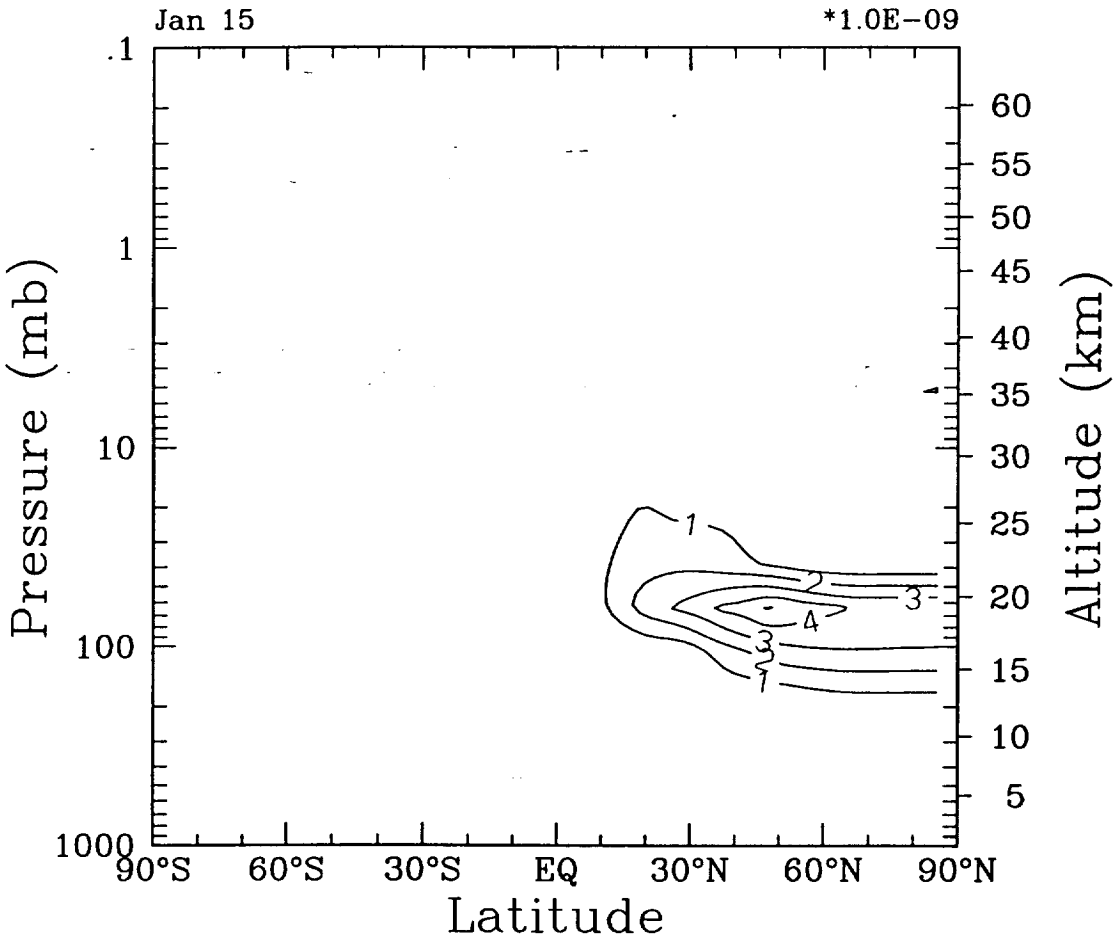

CONTOUR FROM 0. TO 10.000 CONTOUR INTERVAL OF 1.0000 PT(3,31)= 3.42087E-03

Thu Oct 14 10:39:06 EDT 1999

Fig. 6f

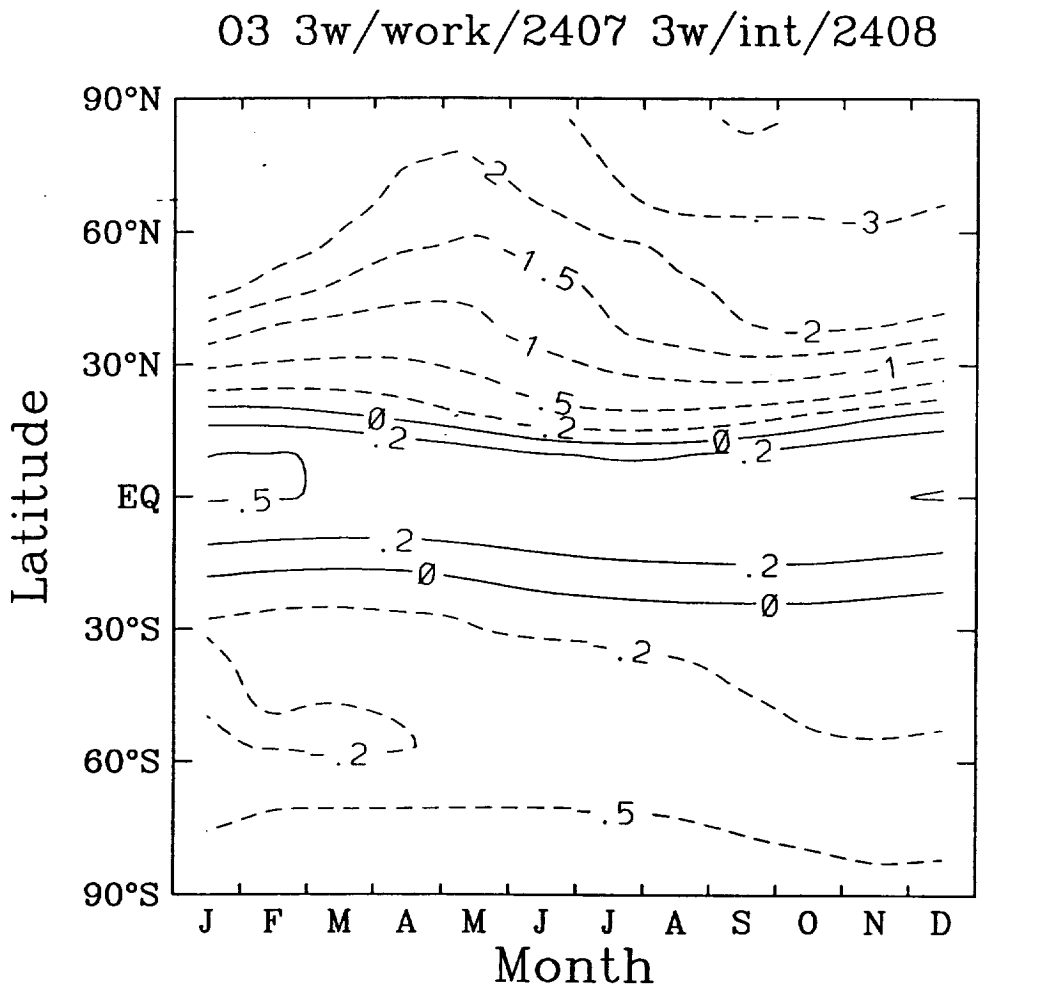

Wed Oct 13 13:34:31 EDT 1999

Fig. 5a

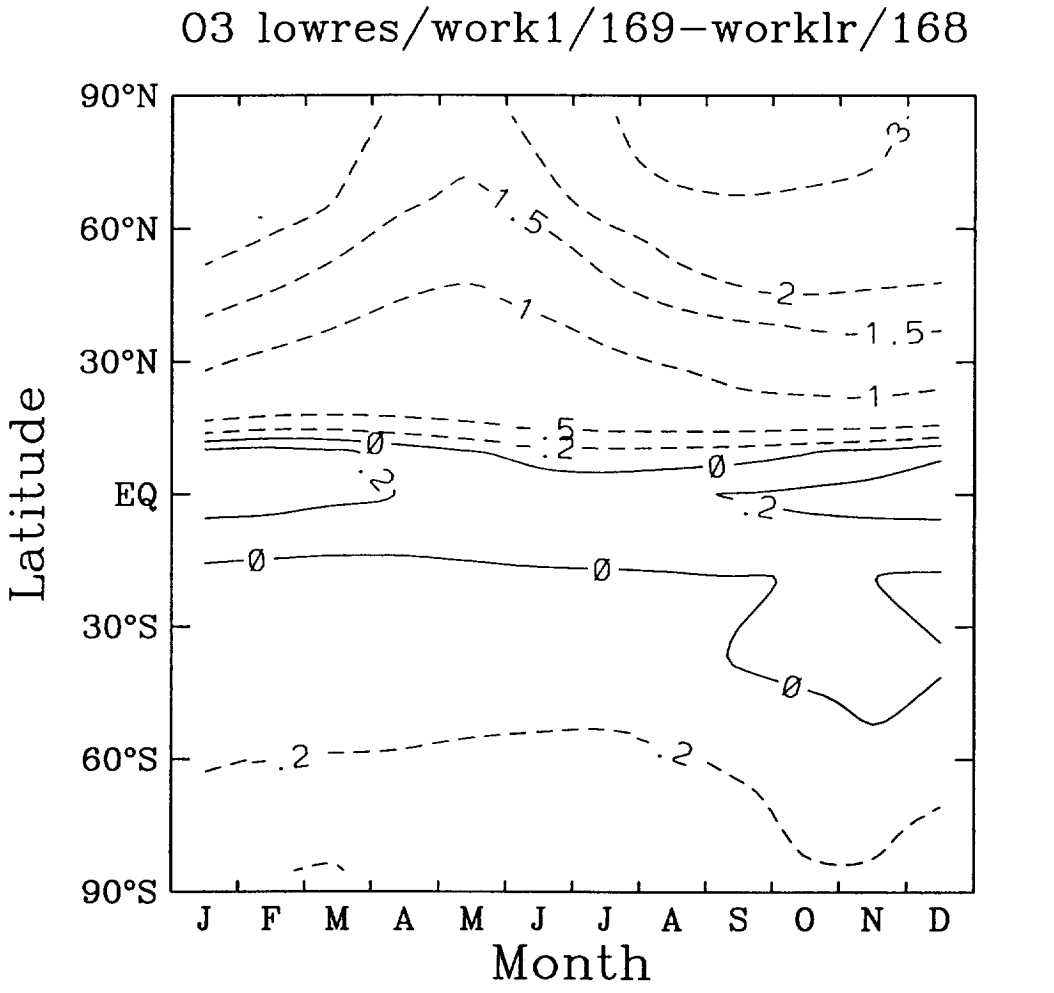

Wed Oct 13 14:02:11 EDT 1999

Fig 5 b

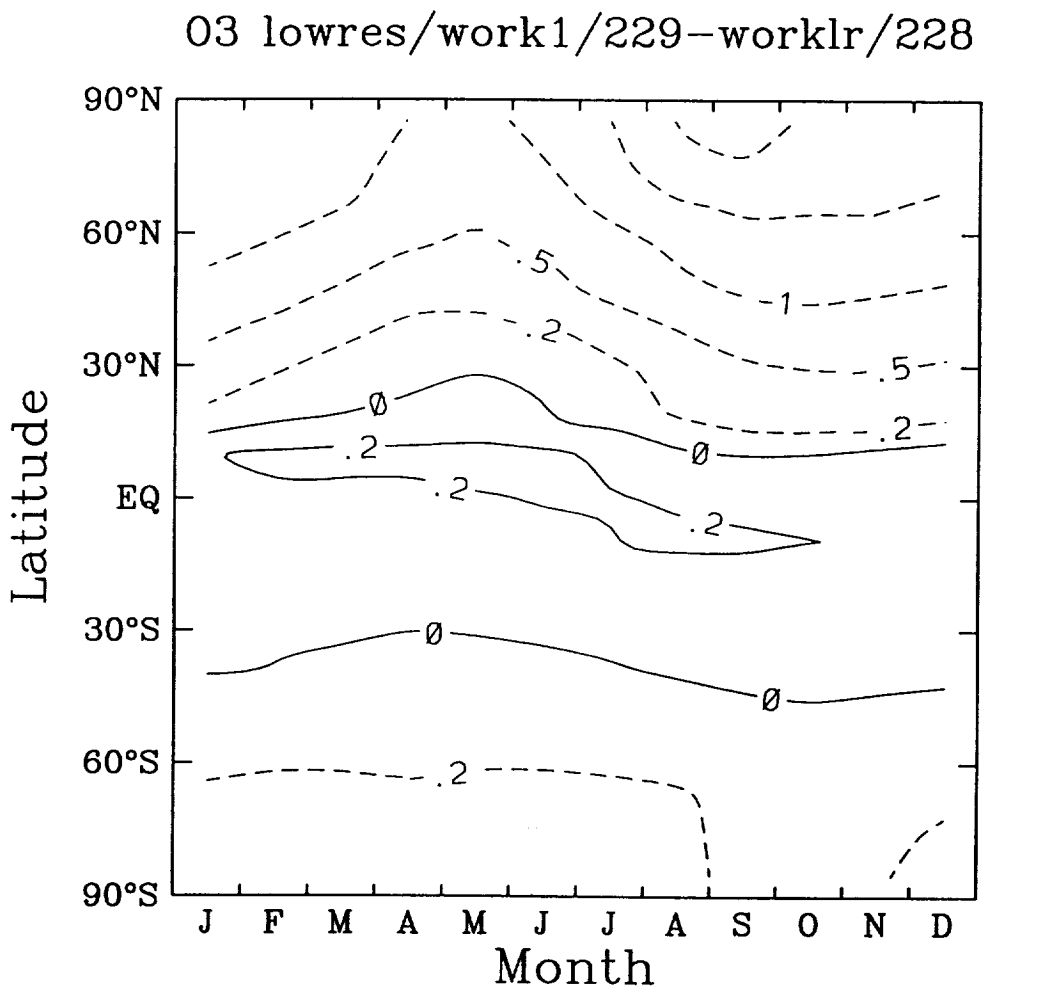

CONTOURS ARE -5.00 -3.00 -2.00 -1.50 -1.00 -0.50 -0.20 0.00 0.20 0.50

Wed Oct 13 14:04:28 EDT 1999

Fig. 5C

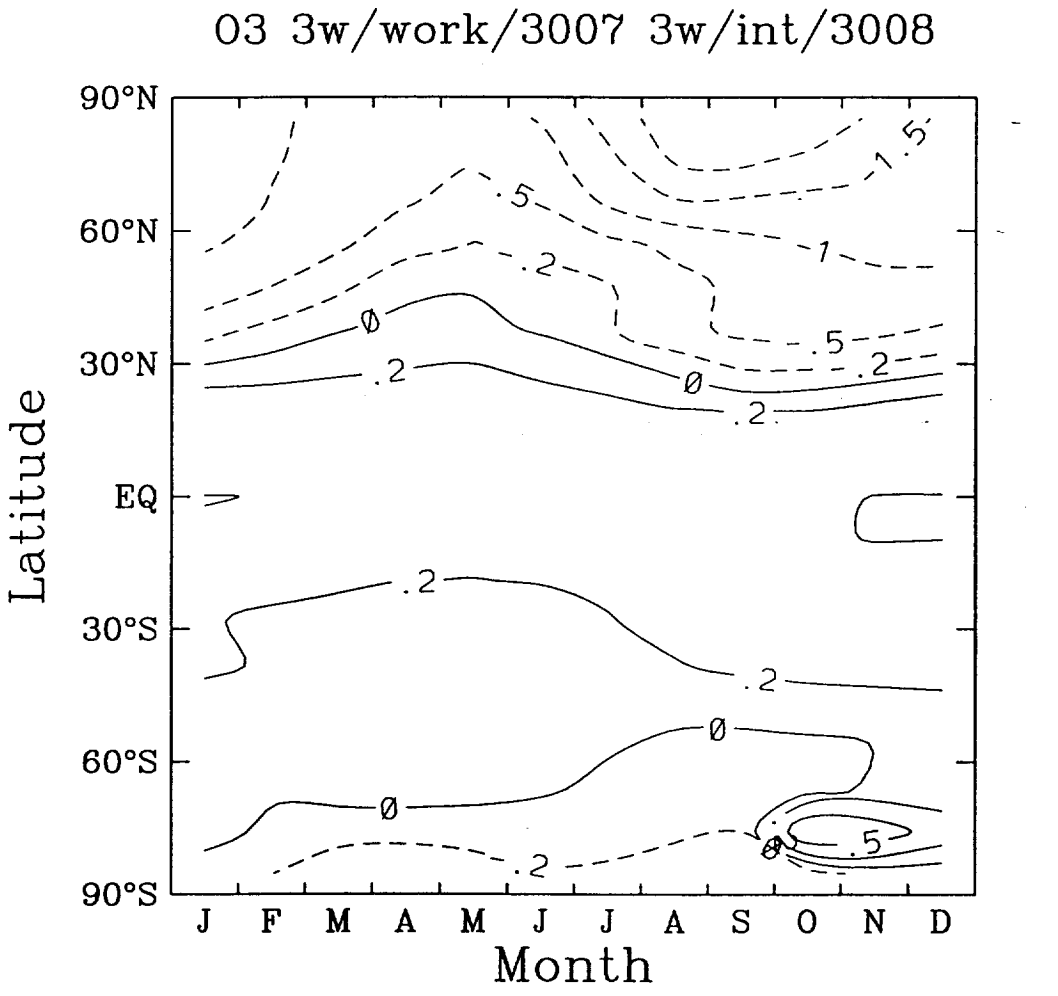

Wed Oct 13 14:05:52 EDT 1999

Fig. 5d

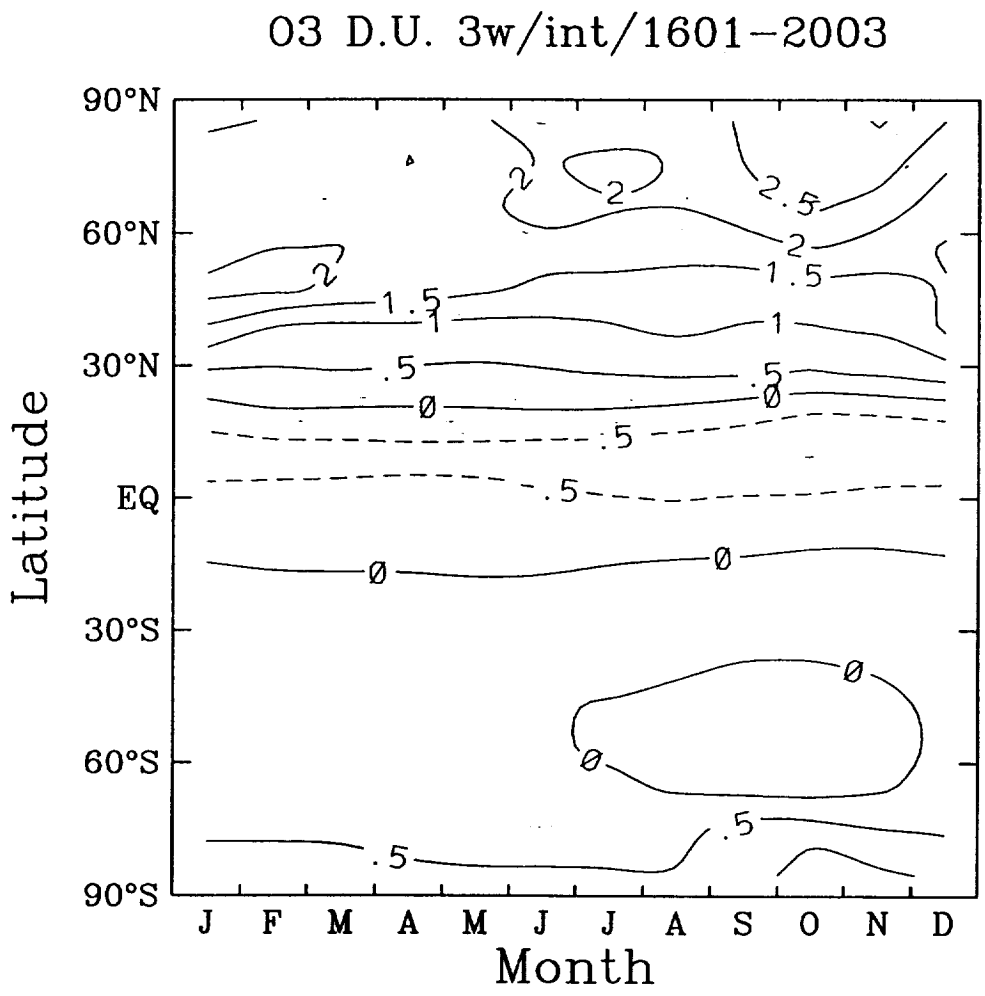

CONTOUR FROM -5.0000 TO 5.0000 CONTOUR INTERVAL OF 0.50000 PT(3,3)= 0.35017

Thu Oct 14 09:03:32 EDT 1999

Fig. 6a

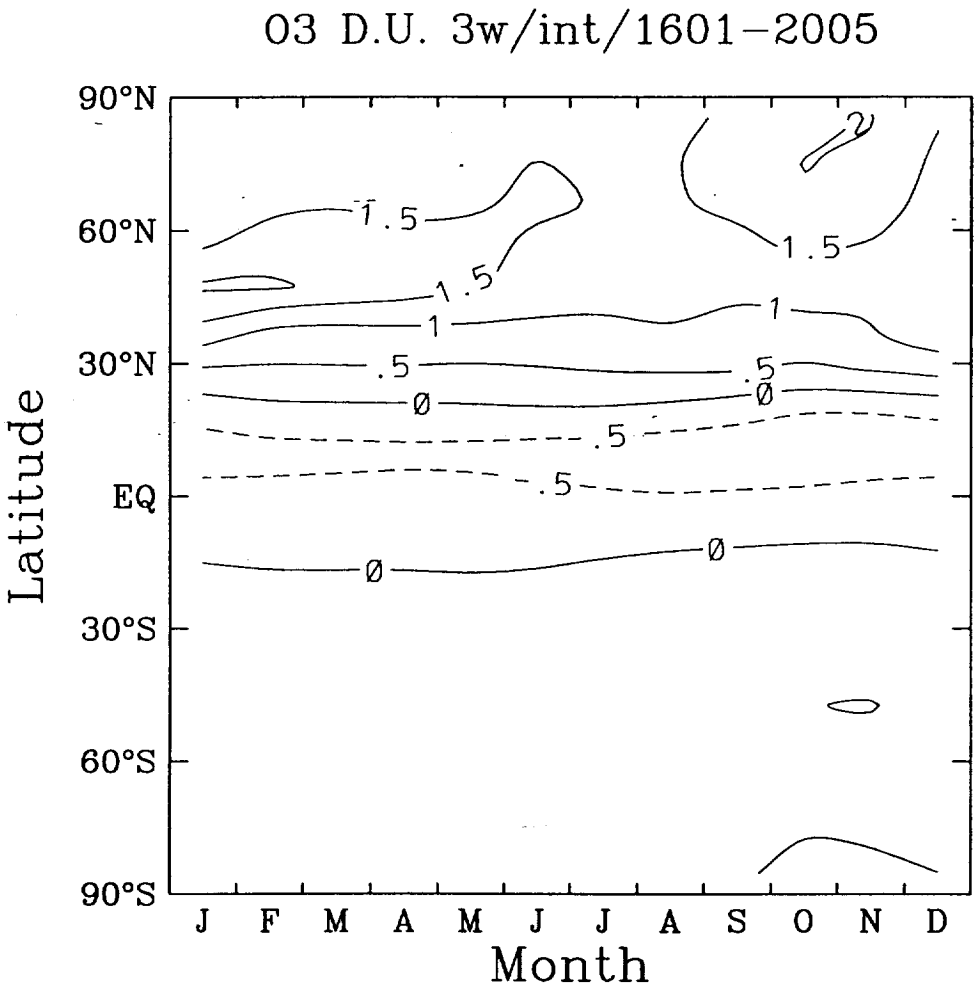

CONTOUR FROM -5.0000 TO 5.0000 CONTOUR INTERVAL OF 0.50000 PT(3,3)= 0.26266

Thu Oct 14 09:02:18 EDT 1999

fig. 66

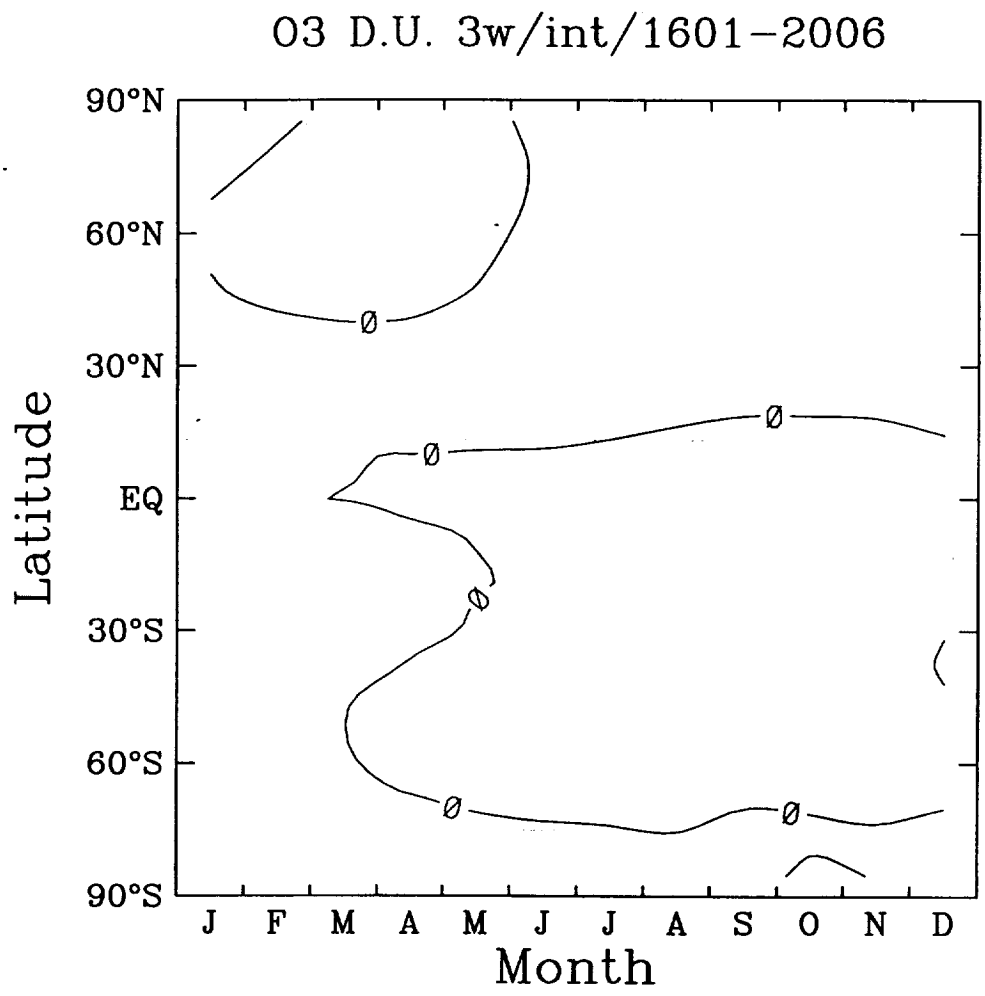
03 D.U. 3w/int/1601-2006
90°N
60°N
30°N
EQ
30°S
60°S
90°S
Latitude
J F M A M J J A S O N D
Month
Ø
CONTOUR FROM -5.0000 TO 5.0000 CONTOUR INTERVAL OF 0.50000 PT(3,3)= 3.37559E-02
Thu Oct 14 09:01:45 EDT 1999

Fig. 6c

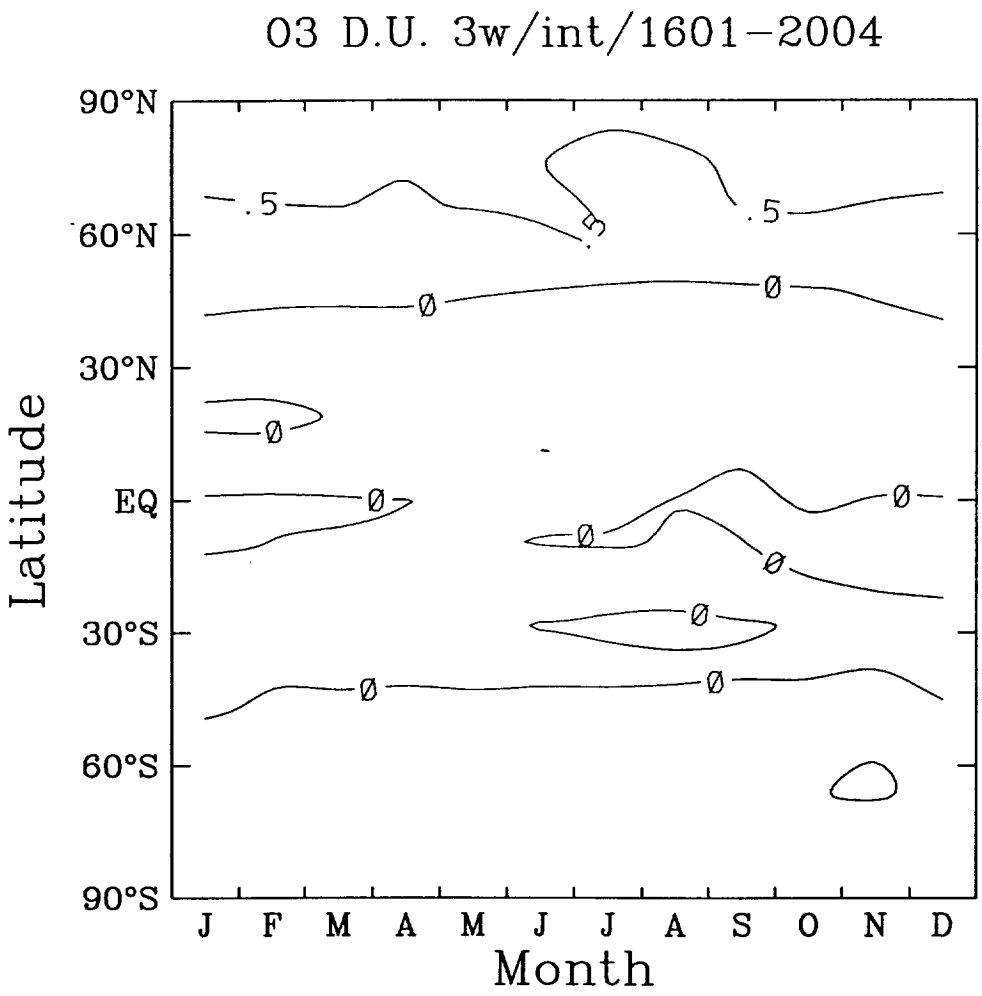

CONTOUR FROM -5.0000 TO 5.0000 CONTOUR INTERVAL OF 0.50000 PT(3,3)= 9.91939E-02

Thu Oct 14 09:02:42 EDT 1999

Fig. 6d